Molecular Dynamics Study of Naturally Occurring Defects in Self-Assembled Monolayer Formation

G. Gannon, J. C. Greer, J. A. Larsson, and D. Thompson*

Tyndall National Institute, University College Cork, Ireland

ARTICLE

ABSTRACT One of the major challenges for nanofabrication, in particular microcontact printing (μ-CP), is the control of molecular diffusion, or "ink spreading", for the creation of nanopatterns with minimized "smudging" at pattern boundaries. In this study, fully atomistic computer simulations were used to measure the impact of naturally occurring domain boundaries on the diffusion of excess alkanethiol ink molecules on printed alkanethiol self-assembled monolayers (SAM). A periodic unit cell containing approximately one million atoms and with a surface area of 56 nm × 55 nm was used to model a hexadecanethiol SAM on Au(111), featuring SAM domain boundaries and a range of concentrations of excess hexadecanethiol ink molecules diffusing on top. This model was simulated for a total of approximately 80 ns of molecular dynamics. The simulations reveal that domain boundaries impede the diffusion of excess ink molecules and can, in some cases, permanently trap excess inks. There is competition between ink spreading and ink trapping, with the ink/SAM interaction strongly dependent on both the ink concentration and the SAM orientation at domain boundaries. SAM defects thus provide potential diffusion barriers for the control of excess ink spreading, and simulations also illustrate atom-scale mechanisms for the repair of damaged areas of the SAM *via* self-healing. The ability of domain boundaries to trap excess ink molecules is accounted for using an accessible volume argument, and trapping is discussed in relation to experimental efforts to reduce molecular spreading on SAMs for the creation of ultrahigh resolution nanopatterns.

KEYWORDS: nanofabrication · microcontact printing (μ-CP) · self-assembled monolayers (SAM) · domain boundaries · molecular dynamics (MD) · molecular diffusion · self-healing

Self-assembled monolayers (SAMs)[1] of alkanethiol molecules binding to gold[2] serve as the prototypical system for studies of soft lithography techniques being explored for applications in nanofabrication.[3] At the boundary of chemistry,[4] biology,[5] and electronics,[6] SAMs offer a versatile platform for nanotechnology.[7] In generating a SAM, alkanethiols can be nanopatterned onto the gold surface using techniques such as dip pen nanolithography,[8,9] high-speed microcontact printing (μ-CP),[10] and edge transfer lithography.[11] Alternatively the entire gold surface can be covered with alkanethiols and the naturally occurring defects used to trap molecular wires.[12,13]

One major bottleneck in the technology transfer of μ-CP to routine use in, for example, commercial lithography processes is the lateral spreading of the excess molecules of the ink used for patterning, where the inks are typically alkanethiols, for example, hexadecanethiol.[14,15] The use of less mobile, heavyweight, and/or multivalent inks can reduce surface diffusion, but possibly at the expense of order and etch resistance of the SAM;[16] for example, heavyweight dendritic inks have recently been used to create sub-100 nm width lines *via* positive μ-CP.[17] More controlled alkanethiol ink diffusion, directed for example by the substrate and/or film topography, may potentially provide routes to the production of patterns with ultrahigh resolution.[14−16]

Experimental microscopy work has shown that SAMs contain a high concentration of defects,[18−22] including those attributable to the underlying gold (grain boundaries, terraces) and those due to the SAM itself (pinhole defects, domain boundaries incorporating gold depressions). Gold grain boundaries are relatively scarce; for example, gold evaporated onto mica has been shown to have gold grains with an area of 280000 square nanometers.[21] In contrast, domain boundaries are unavoidable in alkanethiol monolayer self-assembly and have been shown to have a much smaller area than the gold grains with a typical gold grain containing many SAM domains and their accompanying boundaries.[19,23] Earlier SAM modeling studies[24−27] have been limited due to small simulation cell sizes and/or short sampling times that preclude the treatment of such large-scale SAM structural imperfections and rearrangements.

A detailed picture of the specific excess ink/SAM interactions is difficult to obtain and requires a careful combination of experimental and simulation data.

*Address correspondence to damien.thompson@tyndall.ie.

Received for review December 14, 2009 and accepted January 19, 2010.

Published online January 29, 2010.
10.1021/nn901821h

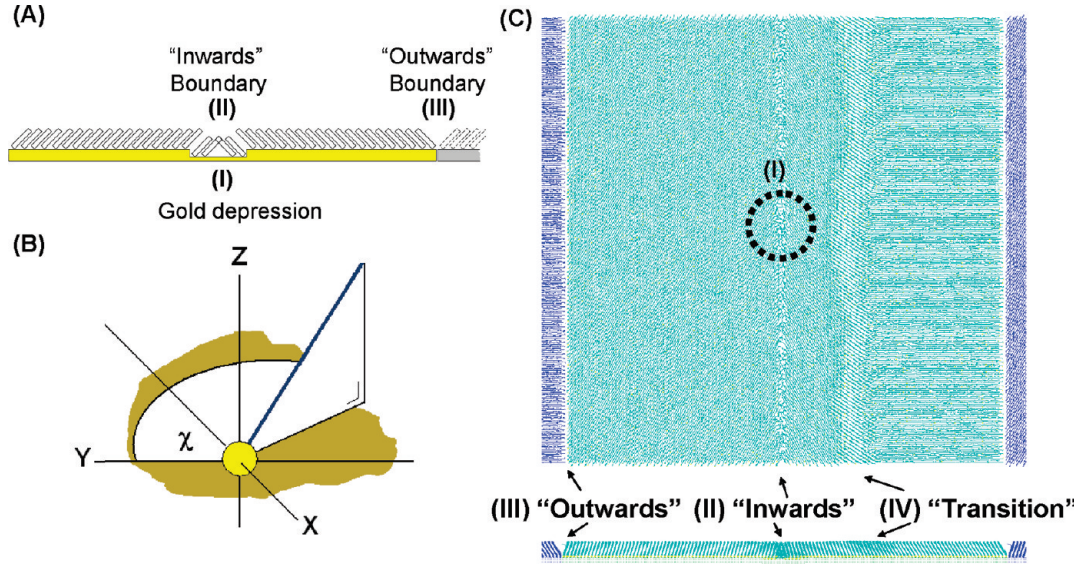

Figure 1. (A) Schematic of a cross-section of the SAM on Au(111), showing the SAM alkanethiol chains as tilted rectangles. Substrate defect (I) and the domain boundaries (II) and (III) are as described in the text; (III) is shown with part of one of the periodic images to illustrate its wedge-like shape. In each case the boundaries are formed by alkanethiol chains with differing interdomain precession angles, χ, as sketched in panel B where χ measures chain precessing about the surface normal *z*-axis projected on to the surface *xy* plane, and the light sphere represents the sulfur atom and the blue line represents the carbon backbone of an alkanethiol chain. Panel C shows a plan and side view of the relaxed 56 nm × 55 nm SAM, prior to the addition of excess ink molecules, with regions labeled as in panel A along with the new "transition" domain boundary (IV), as described in the text. The blue lines to the left and right of the cell are two partial periodic images.

Experiments can be used to estimate overall diffusion rates[10] but the underlying nano- and atom-scale diffusion mechanisms are much more difficult to infer from experiments alone. In the present work we take advantage of the capability provided by highly parallel computing to simulate SAMs on Au(111) structures with over 3000 square nanometers surface area. Simulations of this scale are readily compared to scanning tunneling microscopy (STM) and atomic force microscopy (AFM) images, with atomic-scale resolution retained in the simulations. The simulation cells are large enough to allow explicit treatment of defects in the gold layer and to relate these defects to the structure and dynamics in the SAM.

We find a pronounced dependence of the ink/SAM interaction on local ink concentration, which is known to be dependent on the ink type, concentration, and printing temperatures used in μ-CP experiments,[10,14−16,27] and we discuss these results in relation to experimental imaging studies that highlighted the ubiquity of SAM defects at the nanoscale.[18−20,22,23,28−34] Our molecular dynamics simulations provide atom-scale details of the competition between spreading and trapping of excess ink molecules in SAM formation, which dictates the ultimate pattern resolution attainable from μ-CP. Local excess ink concentration and the atom-scale features of the SAM film also dictate the orientation of trapped molecules, crucial for SAM on gold applications in, for example, molecular electronics.[13,35]

Our principal finding is that naturally occurring SAM film defects can act as barriers to molecular diffusion, providing new data on how excess ink molecules can be integrated into the self-assembling monolayer. Calculated ink spreading and trapping rates exhibit a pronounced dependence on both excess ink concentration and the atom-scale features of the SAM film, paving the way for the directed molecular assembly of more complex pattern geometries using alkanethiols on gold which could potentially provide feature sizes down to 1−2 nm, approaching the regime of truly writing with molecules on surfaces.[16,36] In the shorter term, this new data on the nanoscale mechanisms of SAM self-healing and self-limiting excess ink spreading will aid the identification of optimum processing conditions for μ-CP and show the power of large-scale molecular simulations to complement and deepen experimental knowledge for directed "bottom up" molecular assembly, specifically the optimization of nanopatterning using self-assembly and molecular recognition.

RESULTS AND DISCUSSION

This study employed extensive molecular dynamics computer simulations to describe the fate of excess alkanethiol ink molecules diffusing on top of an alkanethiol SAM on gold featuring naturally occurring substrate and film defects. Our simulation results are described below and discussed in relation to the state of the art in microcontact printing, and will also be of interest to the broader nanofabrication and molecular assembly communities.

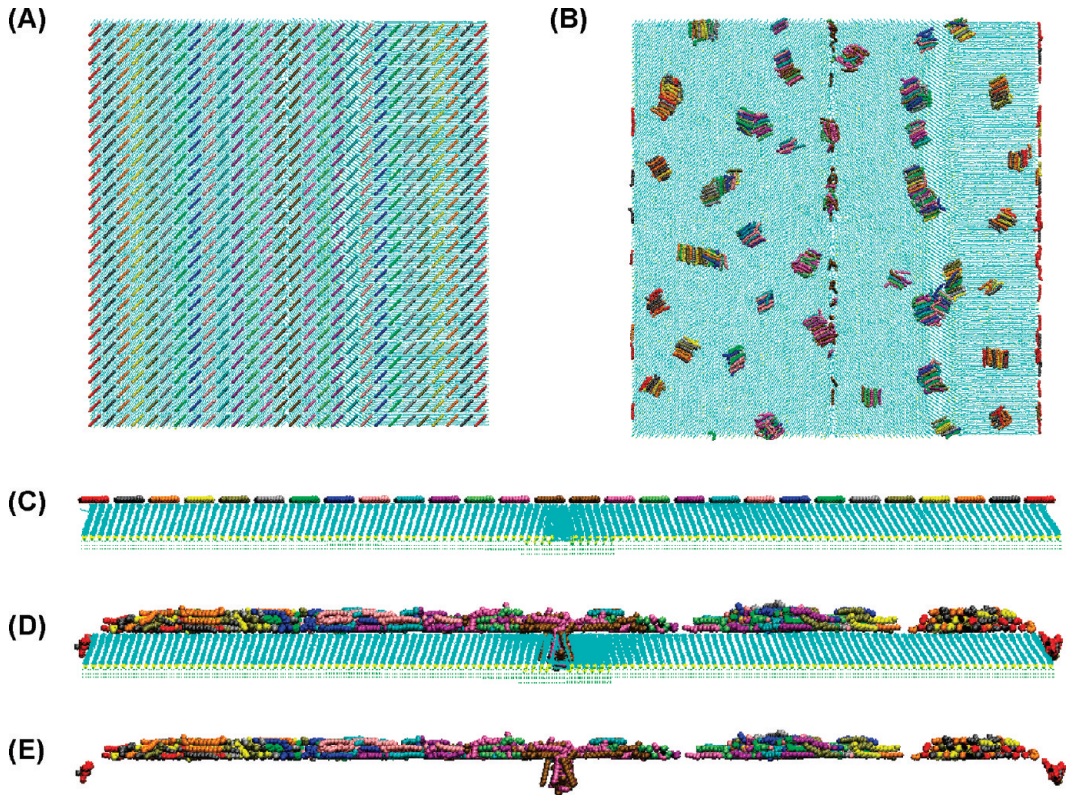

Figure 2. Plan view for the medium excess ink concentration system, showing (A) the initial conformation of excess inks on the relaxed SAM, and (B) the final conformation following 30 ns of free dynamics. Panels C and D give side views of these initial and final conformations; panel E is the same as panel D but with the underlying SAM removed to highlight the trapping. Excess inks of the same color were the same initial distance from the edge of the SAM.

Molecular Trapping at SAM Domain Boundary Defects. The relaxed SAM model formed prior to the addition of excess ink molecules is shown in Figure 1. The SAM modeled here differs, by design, in three respects from an idealized perfect SAM, featuring, as marked in Figure 1, a circular "gold depression" 5 nm wide and 0.249 nm deep, as experimentally found for characteristic defects in the underlying gold substrate in alkanethiol SAMs,[23] together with associated film defects,[18] namely one domain boundary with opposing chains oriented "inwards" towards each other and a second domain boundary with opposing chains oriented "outwards" away from each other. A third "transition" domain boundary arises spontaneously during SAM relaxation, as discussed below in the subsection titled Mobility of the Broad SAM "Transition" Domain Boundary and Temperature Effects. Further technical details on the method and models used can be found in the Materials and Methods section. The large surface area of 56 nm × 55 nm and time scale of ~80 ns used in the simulations permits us to determine the impact of defects on both the SAM structure and the diffusion of excess molecules on top of the SAM. Furthermore, the use of periodic boundary conditions means the model approximates systems of much larger, quasi-infinite area.

Additional unbound alkanethiol molecules were placed on top of the relaxed SAM to model the dynamics of excess ink molecules in SAM formation in, for example, μ-CP. Three excess ink concentrations were considered, which we term low, medium, and high excess ink concentration and which contain 196, 784, and 3136 molecules per cell, respectively, corresponding to excess ink concentrations of 1 molecule per 16, 4, and 1 square nanometer of underlying SAM. The medium excess ink concentration system features a final average excess ink cluster size on top of the SAM of 21 ± 11 molecules (Figure 2), while the low excess ink concentration system forms smaller clusters, with a final average cluster size of 4 ± 3 molecules (Figure 3), and the high excess ink concentration system features much larger, extended ink aggregates, as distinct from discrete clusters (Figure 4). An additional medium excess ink concentration system on an idealized, defect-free SAM was also considered (Figure 5) and had a final average ink cluster size of 17 ± 8 molecules.

For all excess ink concentrations considered some of the excess inks introduced have become trapped in both the "inwards" and "outwards" domain boundaries (Figures 2, 3, and 4). The trapping of excess ink molecules is quantified in Figure 6. Excess molecules within 1.4 nm of the gold surface are considered to be trapped inside the domain boundary; for comparison the termi-

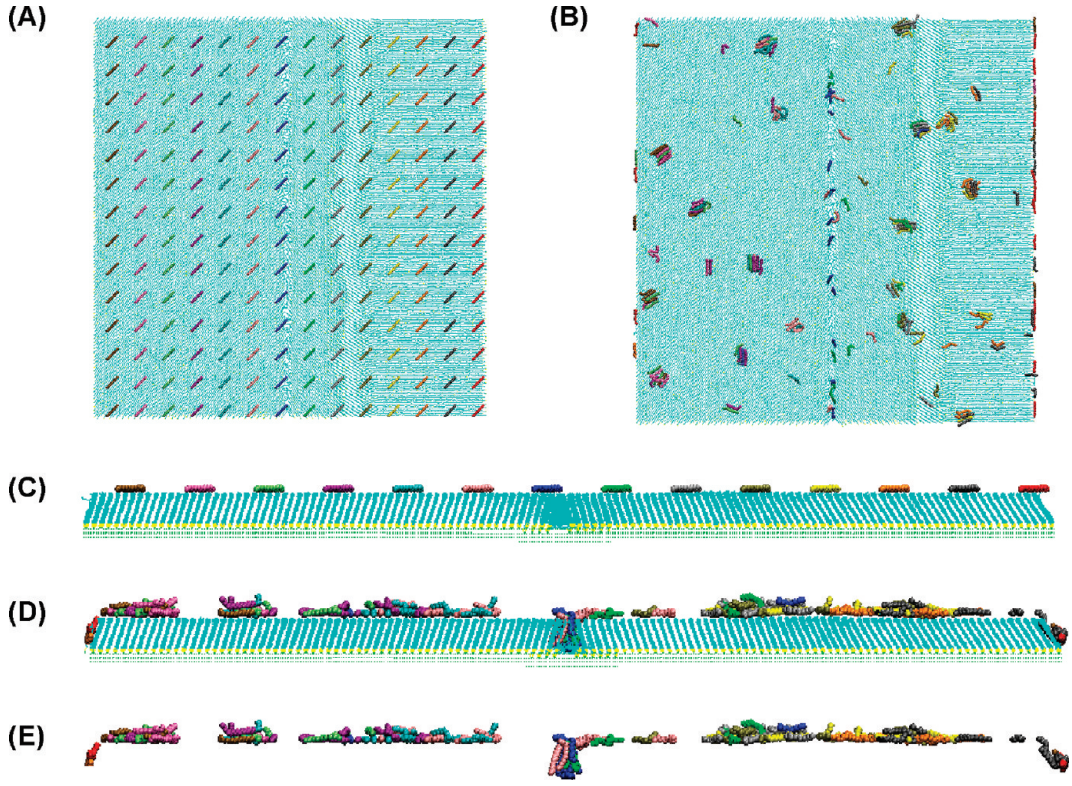

Figure 3. Plan view for the low excess ink concentration system, showing (A) the initial conformation of excess inks on the relaxed SAM, and (B) the final conformation following 17.5 ns of free dynamics. Panels C and D give side views of these initial and final conformations; panel E is the same as panel D but with the underlying SAM removed to highlight the trapping. Excess inks of the same color were the same initial distance from the edge of the SAM.

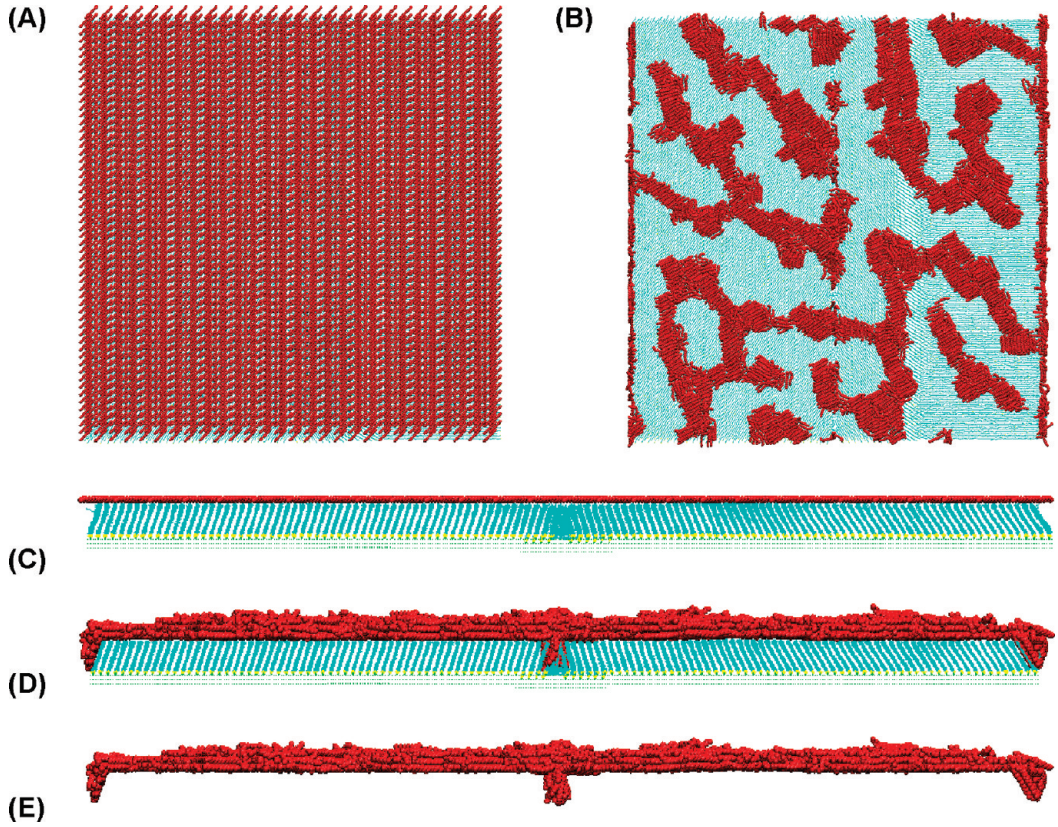

Figure 4. Plan view for the high excess ink concentration system, showing (A) the initial conformation of excess inks on the relaxed SAM, and (B) the final conformation following 10 ns of free dynamics. Panels C and D give side views of these initial and final conformations; panel E is the same as panel D, but with the underlying SAM removed to highlight the trapping.

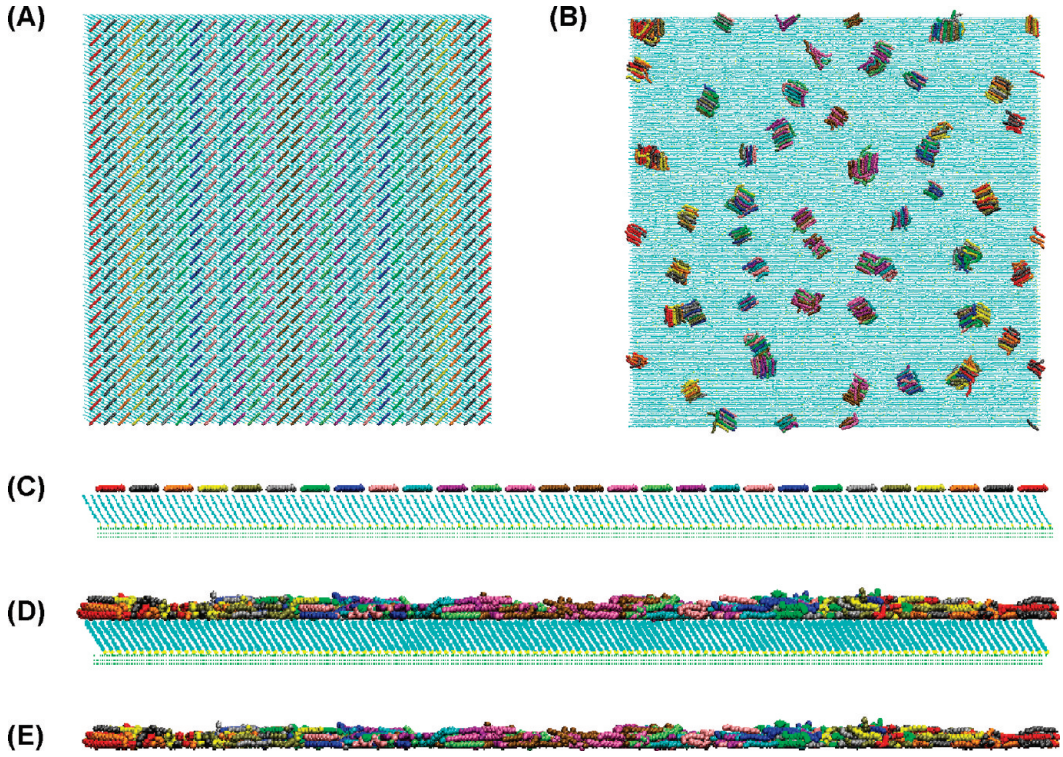

Figure 5. Plan view for the medium excess ink concentration on an idealized, defect-free SAM, showing (A) the initial conformation of excess inks on the SAM, and (B) the final conformation following 17 ns of free dynamics. Panels C and D give side views of these initial and final conformations; panel E is the same as panel D but with the underlying SAM removed to highlight, in this case, the absence of trapping. Excess inks of the same color were the same initial distance from the edge of the SAM.

nal, methyl carbons of the bound SAM alkanethiol chains are approximately 2 nm above the gold surface. Figure 6 shows that the number of trapped excess molecules increases rapidly within the first few nanoseconds, after which the rate of trapping decreases. The number of trapped excess molecules only very occasionally drops, indicating that excess molecules that diffuse into a domain boundary are effectively trapped. Furthermore, approximately half the excess molecules trapped in near-vertical orientations in the "inwards" domain boundary are found with the sulfur atoms pointing toward the gold. It is worth remembering that the analytical potentials used in the molecular dynamics are incapable of describing covalent bond formation; those excess molecules with the sulfur in the vicinity of the gold surface are expected to bind to the gold under normal experimental conditions[37,38] and become permanently incorporated into the SAM.

Using the medium excess ink concentration system as a reference and comparing the three systems after 10 ns, quartering the concentration of excess inks (comparing the medium and low ink concentrations) reduces by half the number of excess inks trapped in the "inwards" domain boundary. On the other hand quadrupling the excess ink concentration (comparing the medium and high ink concentrations) increases the number of excess inks trapped in the "inwards" domain boundary by a factor of 1.5. At the "outwards" domain boundary quartering the excess ink concentration (comparing the medium and low ink concentrations) reduces the number of excess inks trapped by one-third, while quadrupling the excess ink concentration (comparing the medium and high ink concentrations) greatly increases the number of excess inks trapped by a factor of 6. From the structures given in Figure 4, it is clear that the "outwards" domain boundary is effectively saturated with excess ink molecules at the high excess ink concentration. This provides an upper limit for excess ink trapping at this type

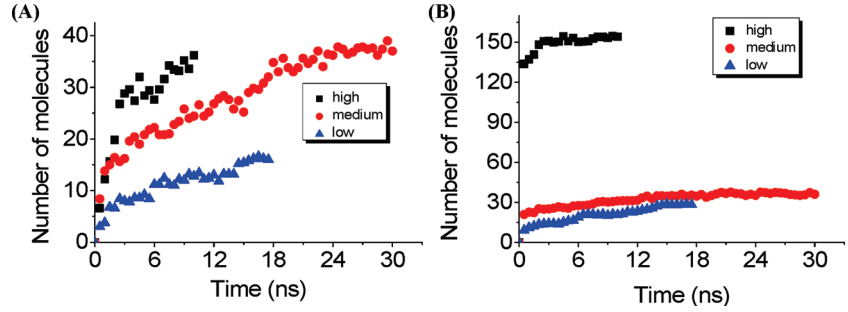

Figure 6. The number of excess ink molecules trapped at the (A) "inwards" and (B) "outwards" domain boundary at the three different excess ink concentrations (low, 196 molecules; medium, 784 molecules; and high, 3136 molecules) as a function of time.

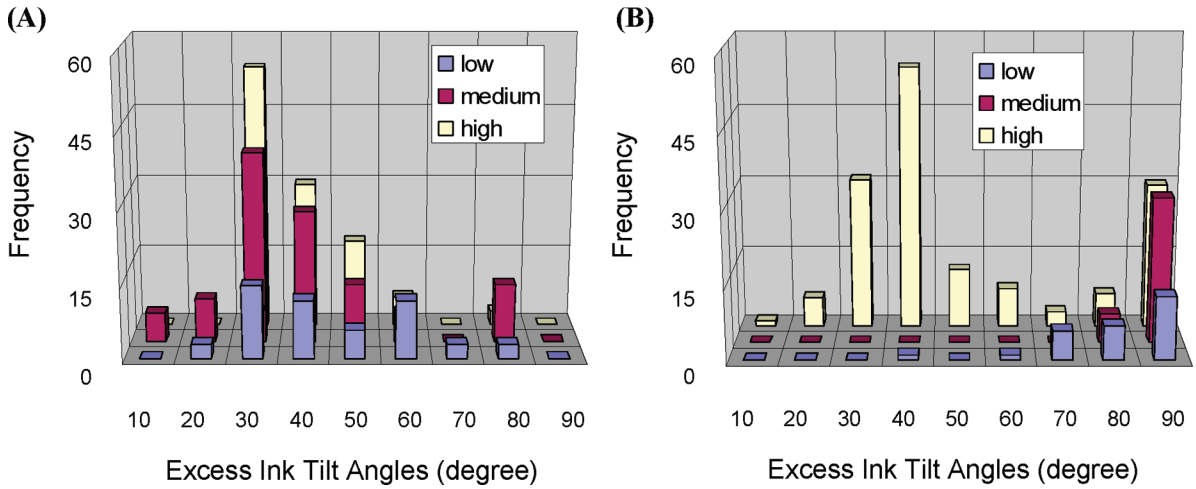

Figure 7. Tilt angle distributions for excess ink molecules trapped in the (A) "inwards" and (B) "outwards" domain boundary at the three different excess ink concentrations (low, 196 molecules after 17.5 ns; medium, 784 molecules after 30 ns; high, 3136 molecules after 10 ns).

of boundary of approximately 1.4 excess inks per square nm of SAM surface area, defining the SAM surface area as simply the base of the wedge shape formed by the "outwards" domain boundary. Figures 2 and 3 show, on the other hand, that neither the "inwards" nor "outwards" domain boundary is saturated for the low and medium ink concentrations, suggesting that diffusion at longer times to these regions will result in further trapping. This is supported by the enhanced trapping observed in simulations performed at elevated temperature, as described in subsection Mobility of the Broad SAM "Transition" Domain Boundary and Temperature Effects below.

Atom-Scale Mechanisms for Ink Incorporation into the SAM at Low, Medium, and High Excess Ink Concentrations. The orientation of alkanethiol molecules trapped in the "inwards" domain boundary is shown in Figure 7A. The spread in the data reflects the range of tilt angles that the trapped excess molecules can adopt. For example, some of the trapped excess molecules are lying almost parallel to the surface as indicated by the presence of tilt angles around 80° and 90°. Nevertheless there is a peak in all the tilt angle distributions at 30°. The significance of the 30° tilt angle is that this is the tilt angle of the bound SAM chains.[1,27] Therefore excess molecules can flow into the "inwards" domain boundary defect and orient themselves in the same arrangement as the bulk SAM. The trapped excess molecules are effectively healing the defect by filling the boundary between the domains.

In contrast to the similarity in tilt angles for excess inks trapped in the "inwards" domain boundary, the tilt angles for excess inks trapped in the "outwards" domain boundary display a pronounced dependence on concentration, as shown in Figure 7B. In the lower concentration systems (the 196 and 784 excess ink systems) most of the trapped excess alkanethiol inks lie parallel to the surface as shown by the predominant peak centered at 90°. On the other hand, in the higher concentration, 3136 excess ink system, most of the trapped excess inks are standing up as evidenced by the large populations at 30−40°. Interestingly these changes in tilt angle mirror the growth of an alkanethiol SAM, where during SAM formation the alkanethiols initially lie parallel to the surface at low concentrations and as the concentration increases they stand up to adopt a near 30° tilt angle.[39] Furthermore, whereas the molecules on the surface cluster (Figures 2−5), this does not happen to the molecules in the "outwards" domain boundary. This can be interpreted as the excess ink molecules changing from a partial wetting of the surface to a more complete wetting of the wedge-shaped "outwards" domain boundary.

Even longer simulations would be needed to ascertain whether the "inwards" domain boundary is completely or only partially healed by molecular trapping and so unhealed "inwards" domain boundaries may or may not remain at experimental time scales. Conversely, the "outwards" domain boundary, though filled with excess molecules, has no free surface gold sites (as sketched in Figure 1) to permanently bind excess molecules and so may be expected to contribute strongly, along with the substrate defects, to the high density of narrow "cracks" in SAM microscopy images.[1,18−23,30,32,40,41]

Effect of Domain Boundaries on Calculated Excess Ink Spreading Rates. Calculated excess ink diffusion coefficients for the medium ink concentration system are plotted as a function of time in Figure 8A, with diffusion coefficients on a reference idealized, defect-free SAM also shown for comparison. It takes at least 8 ns for the diffusion coefficient to reach a steady-state value, emphasizing the need for long simulation times

to develop an accurate picture of excess ink dynamics on the surface of the SAM. Figure 8A shows that as time progresses the self-diffusion coefficient drops sharply as ink molecules cluster on top of the SAM (Figures 2 and 5) before eventually reaching a value of $(2.7 \pm 0.3) \times 10^{-6}$ cm^2 s^{-1} (averaged over the last 15 ns). The calculated self-diffusion coefficient is hence approximately twice the computed self-diffusion coefficient of bulk liquid hexadecanethiol,[27] which is equal to 1.3×10^{-6} cm^2 s^{-1}. Hence two-dimensional self-diffusion at lower concentrations proceeds on a faster time scale than the similar process in the bulk.

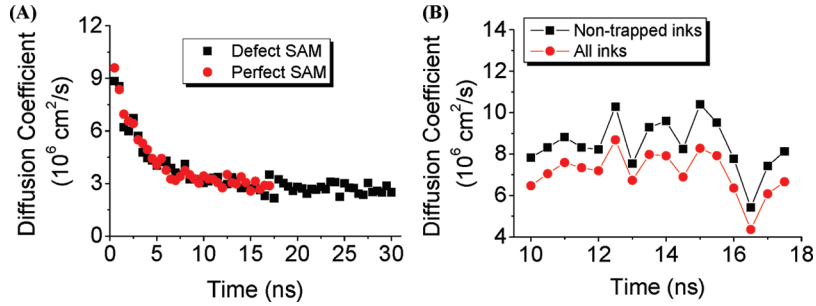

Figure 8. (A) Computed excess ink diffusion coefficients for the medium excess ink concentration system over 30 ns, with coefficients computed over 17 ns on a reference idealized, defect-free SAM also given for comparison. (B) A comparison of the computed excess ink diffusion coefficients for all inks, and just nontrapped inks, in the low ink concentration system illustrating how a high percentage of trapped ink, in this case over 20% (see text), gives a quantifiable reduction in ink diffusion.

The final percentage of excess inks trapped at the three concentrations is 22.5%, 9.3%, and 6% for the low (after 17.5 ns), medium (after 30 ns), and high (after 10 ns) concentration systems, respectively. Hence, as shown in Figure 8A, for the medium concentration system, the difference in computed diffusion coefficients for the defect and perfect SAMs is very small, reflecting the very low percentage of trapped excess inks. Similarly for the higher concentration system, the low percentage of trapped excess inks is attributable to the saturation of the "outwards" domain boundary shown in Figure 4. At the lowest excess ink concentration a higher fraction of the inks, over 20%, have become trapped, and so this system exhibits a measurable decrease in the self-diffusion coefficient generated for all its excess inks compared to the self-diffusion coefficient generated for just the nontrapped excess inks, as shown in Figure 8B. Hence, as the fraction of trapped excess inks increases, SAM defects exhibit a progressively stronger influence on excess ink spreading.

The simulations show then how domain boundary defects in the SAM film can trap excess molecules; the single gold depression defect on the other hand (*cf.* Figure 1) did not have a measurable influence on trapping. Taking for example the medium ink concentration system, film defects trapped almost 10% of the excess molecules by the end of the simulation at 30 ns, with approximately 2.5% of the excess molecules—half the molecules trapped in the "inwards" boundary—expected to covalently bond to the gold substrate and so become permanently incorporated into the SAM. Experimentally approximately 30 gold depressions and 10 distinct domains have been observed in a similarly sized area, 50 nm × 50 nm.[19] As the concentration of defects increases it is reasonable to assume that trapping and SAM self-repair will increase, giving reduced smudging at pattern edges as molecular spreading on the SAM is further inhibited. More generally, diffusion coefficients of nontrapped excess inks diffusing on top of the SAM generally increase at lower excess ink concentrations, reflecting the higher proportion of more mobile smaller ink clusters and also highly mobile nonclustered single ink molecules.[27] Overall, the competitive spreading and trapping mechanisms exhibit a complex dependence on excess ink and SAM defect concentrations (with these concentrations also coupled and interdependent), and so measured spreading rates will be an ensemble average based on a large number of kinetically weighted nanoscale ink/ink and ink/SAM interactions.

Mobility of the Broad SAM "Transition" Domain Boundary and Temperature Effects. As shown in Figure 1 above, a broad "transition" region arises spontaneously on the right-hand side of the SAM during the initial SAM relaxation phase prior to the addition of the excess ink molecules, thereby breaking the symmetry of the model. Interestingly, similar sized broad "transition" regions between individual domains of alkanethiol SAMs on Au(111) have been recently recorded using very high resolution force microscopies.[23,32] AFM indicates that these approximately 5 nm wide boundaries have alkanethiol coverage commensurate with that of the rest of the SAM,[23] while friction force microscopy (FFM) revealed 5−10 nm broad interdomain regions in lateral force profiles.[32] A proposed mechanism for the broad "transition" domain boundary formation may be found in Supporting Information. The broad "transition" regions are not to be confused with the many, sharp lines or "cracks" of a few-nm wide which have long been observed in microscopy experiments[19,30,32,41] which are generally attributed to a range of both substrate and film imperfections. In the present simulations these sharp cracks correspond to the narrow central "inwards" and edge "outwards" domain boundaries, in particular the "outwards" domain boundary would give a sharper decrease in terminal methyl height and thus produce the experimentally observed distinct black lines.

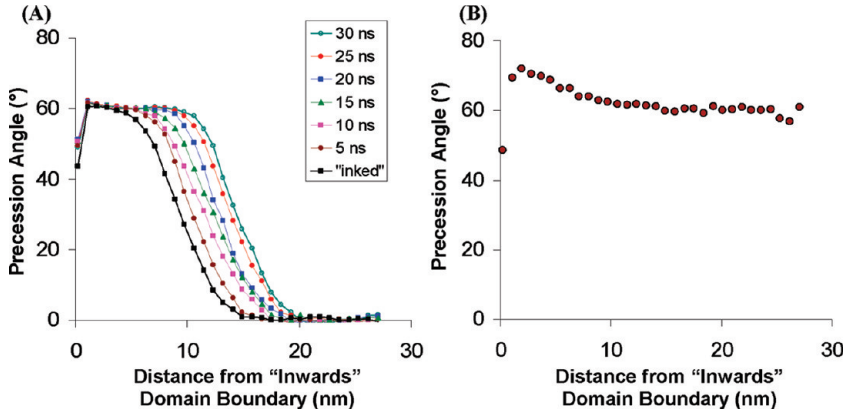

Figure 9. SAM precession angle distribution from the "inwards" domain boundary to the "outwards" domain boundary, corresponding to the right-hand side of Figure 1. Panel A shows the distribution at seven different time segments, starting from the "inked" SAM generated immediately following the initial (bare) SAM relaxation, as described in the text. The shift in the distribution highlights the movement of the broad "transition" region, and panel B shows the distribution following 5.5 ns of simulated high-temperature dynamics at 383 K.

Film precession and tilt angle distributions in the relaxed SAM, prior to the addition of the excess ink molecules, are given in Supporting Information. Figure 9A shows a plot of the precession angles of the right-hand side of the SAM (using the orientation shown in Figure 1) at seven different times during the long ink-on-SAM simulations, indicating that the broad "transition" region moves toward the "outwards" domain boundary over the course of the 30 ns simulation. As a first approximation to longer time dynamics, we performed also a high-temperature simulation which suggests that it may be possible to anneal out the broad "transition" region. Note that the combination of short sampling time of ~5 ns and very high temperature of 383 K were chosen to provide *simulation* conditions that (a) avoid complete disordering of the SAM film while (b) allowing large-scale domain relaxation not accessible within the ~30 ns sampling time at room temperature; in experiments, such elevated temperatures would cause chain desorption in the SAM and also

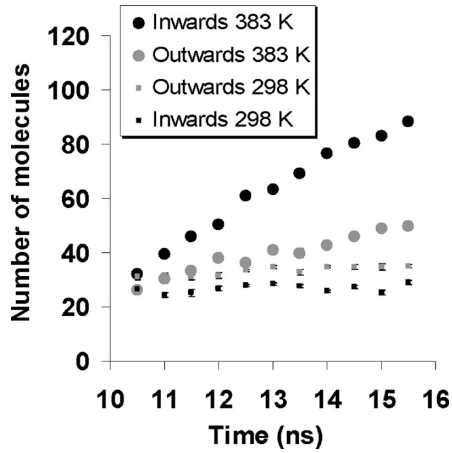

Figure 10. . The number of excess ink molecules trapped at both the "inwards" and "outwards" domain boundary of the medium excess ink concentration system at 298 and 383 K as a function of time.

widespread diffusion of gold atoms in the substrate.[1] Further simulation and experimental studies, beyond the scope of the present work, would be required to show conclusively whether or not the broad domain boundaries observed[23,32] at experimental time scales correspond to the mobile film "transition" regions formed in our simulation model.

In addition to the rearrangements within the SAM film, Figure 10 shows that increasing the temperature increases molecular trapping at both the "inwards" and "outwards" domain boundaries. This increased trapping can be explained by considering that the excess inks are more mobile at higher temperature and consequently more excess inks arrive at the domain boundaries. Note also that Figure 9B shows that the precession angles close to the "inwards" domain boundary have shifted above 60° thereby further increasing the volume available for trapping, as explained in subsection An Explanation for Excess Ink Trapping Based on SAM Accessible Volume below. On the contrary, the change in precession angle from 0° to 60° at increased temperature (Figure 9) results in *decreased* accessible volume at the "outwards" domain boundary, and so although the number of excess inks trapped at the "outwards" domain boundary increases at higher temperature due to increased ink mobility, trapping does not increase as much as at the "inwards" domain boundary due to the decrease in SAM accessible volume. This concept of "ink-accessible volume" in the SAM is developed further below.

An Explanation for Excess Ink Trapping Based on SAM Accessible Volume. Figure 11 illustrates the SAM accessible volume available for molecular trapping at different domain boundaries. In sketching the different interfaces, the central arrangement (d) represents a single domain in which there is no difference in precession angles between alkanethiol chains comprising the domain, that is, deep within a domain and away from the boundary, imitating the idealized, defect-free SAM geometry. In arrangements c, b, and a, there is a progressively larger increase in volume between the two chains, whereas in arrangements e, f, and g, there is a progressively larger decrease in volume between the two chains. It is observed that within a domain, with all SAM chains adopting the same precession angle, as represented in arrangement d, there is no trapping of excess ink molecules, as shown in Figure 5 above. The lack of trapping at the broad "transition" domain boundary, which corresponds to arrangement e in Figure 11, is thus due to its packing arrangement, with even less accessible volume available than in the

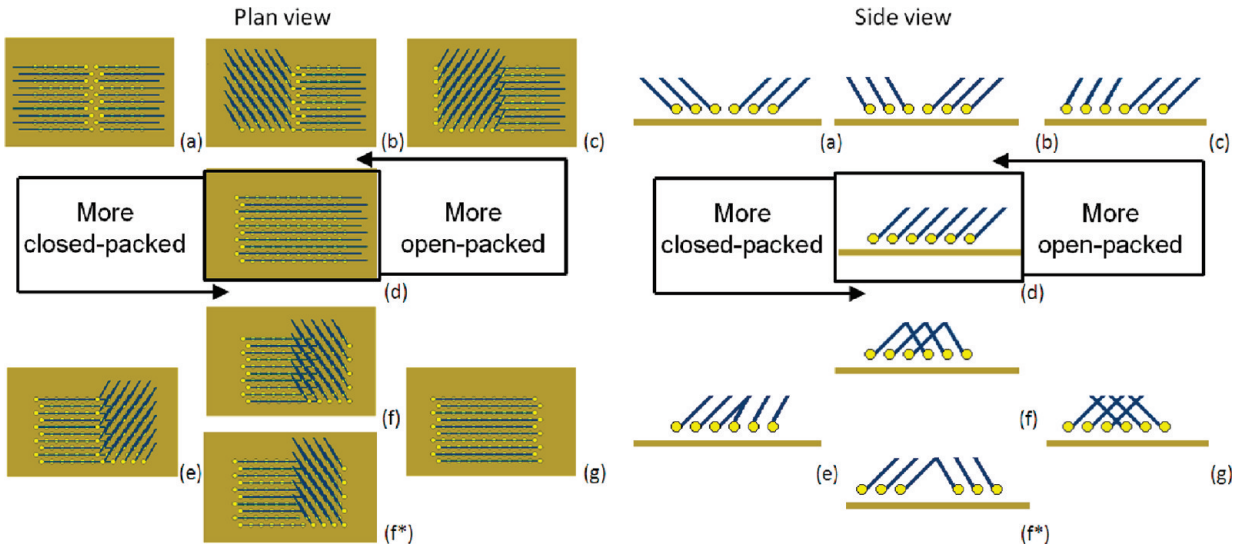

Figure 11. Possible precession angle-based interfaces between two SAM alkanethiol chains shown in (left) plan and (right) side views. The light spheres represent the sulfur atoms and the dark lines represent the alkanethiol chains. The possible arrangement of precession angles are (a) two alkanethiols with precession angles in opposite, 180° separated, directions; (b) the alkanethiol on the left is rotated through a precession angle of 60°, equivalent to the "outwards" domain boundary; (c) the alkanethiol on the left is rotated through a further precession angle of 60°, approximated by the high temperature "outwards" domain boundary described in the text; (d) the alkanethiol on the left is rotated through a final precession angle of 60°, the precession angles now match, corresponding to two rows of noninterfacial alkanethiol chains within a domain; (e) the alkanethiol chain on the right is rotated through a precession angle of 60°, equivalent to the broad "transition" boundary; (f) the alkanethiol on the right is rotated through a precession angle of a further 60°, similar to the "inwards" domain boundary sketched explicitly in panel f*; and finally, (g) the alkanethiol on the right is rotated through a final 60°, the two alkanethiol chains now directly opposing each other in an unphysical arrangement included here for the sake of set completion.

defect-free regions of the SAM. Similarly, the unphysical arrangements f and g, included here for the sake of set completion, would also be too close-packed to act as ink traps.

Trapping at the "inwards" domain boundary can be attributed to its construction (*cf.* Figure 1). Two groups of opposing chains meet with the chains oriented as sketched in the Figure 11f arrangement but with a reduced SAM chain concentration at the boundary to give the physical interface sketched in panel f*. The "outwards" domain boundary, sketched in Figure 11 as interface b, also traps excess ink molecules. It is to be expected then, that when the volume between SAM alkanethiol chains is further increased, as in Figure 11 arrangement a, that it too would trap excess molecules. Similarly, the interface shown in Figure 11 as arrangement c is more open-packed than the nondefect regions and so may act as a trap. Although the room temperature stability of the arrangements sketched in panels a and c of Figure 11 has not been tested, an arrangement similar to panel c formed in the high temperature simulations described above in subsection Mobility of the Broad SAM Transition Domain Boundary and Temperature Effects. The trapping ability of all possible alkanethiol chain interfaces, as given in Figure 11, has thus been addressed, either explicitly from simulation, arrangements b, d, e, and f*, or by implication, a, c, f, and g. Finally, molecular dynamics snapshots of the three domain boundary interfaces are given in Figure 12, illustrating the change in SAM precession angle and ink-accessible volume at each interface. The "inwards" and "outwards" domain boundary feature SAM

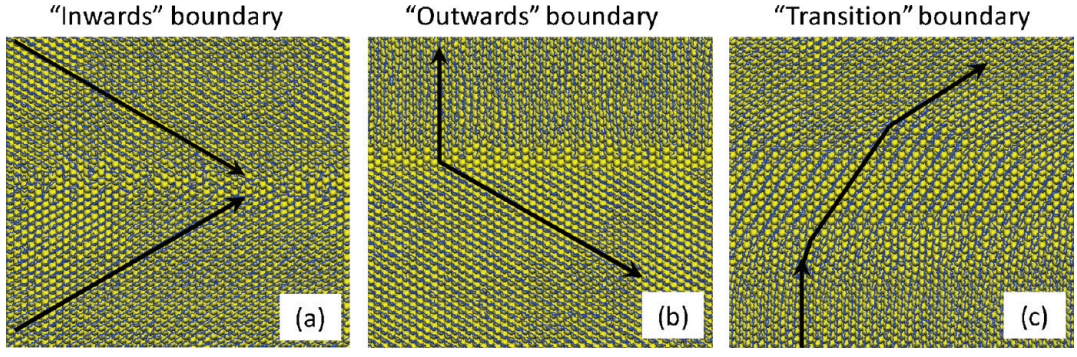

Figure 12. Simulation snapshots illustrating the three precession angle-based domain boundaries, in plan view. Gold atoms are shown as spheres and the SAM alkanethiol chains are shown as lines. The large black arrows emphasize the direction of the chains.

chain interdigitation and a wedge-like shape, respectively, while the "transition" boundary is too tightly packed to trap molecules.

CONCLUSIONS

Fundamental insights have been obtained into nanofabrication using SAMs, made possible by massively parallel computer simulations with on the order of one million atoms and a combined/total simulation time approaching 0.1 microseconds. The simulations reveal several important features of the dynamics of SAM formation at short time scales (in the experimental context). Domain boundaries are ubiquitous, and are often associated with substrate defects as well as transitions between molecular domains with different SAM chain orientations. Interestingly for the application of SAMs on gold in nanofabrication and production of reproducible nanopatterns with few-nanometer feature sizes, we find that strong molecule-SAM interactions occur at SAM domain boundaries, competing with molecule−molecule clustering on top of the SAM. Domain boundaries can trap excess molecules, with trapped excess molecules adopting different orientations in different SAM domain boundaries, leading to SAM self-healing and repair in some instances.

Excess molecular ink spreading is one of the limitations of nanopatterning, in particular μ-CP. Furthermore, recent variants of the standard μ-CP technique such as microdisplacement printing[42] and microcontact insertion printing[43] rely on the addition of ink molecules to an existing SAM. Some types of features written with dip pen nanolithography also require controlled diffusion of ink molecules on a preexisting pattern.[8,9] It is striking then that naturally occurring SAM imperfections may play a beneficial role by controlling the spreading of excess ink molecules and so reducing "smudging" at pattern boundaries.

While experiments provide a wealth of data on structure, dynamics and overall energetics they often miss the underlying, often very complex and numerous, nanoscale events that contribute to the observed assemblies, limiting the usefulness of stand-alone experimental data for material/process optimization. To date, quantitative data has been lacking on the influence of substrate and film defects on SAM formation. In the present work, computer simulations provided atom-scale information on defect-associated SAM relaxations and trapping of excess molecules, providing heretofore inaccessible data on domain evolution as well as SAM repair and self-healing crucial for the use of SAMs in ultrahigh resolution nanofabrication.

MATERIALS AND METHODS

The SAM model features 14112 hexadecanethiol molecules self-assembled on Au(111), with molecules arranged according to a c(4 × 2) unit cell,[1] generating a system with surface dimensions of 56 nm × 55 nm and containing 834624 atoms. The alkanethiol starting tilt angles were set close to the experimentally measured tilt angle of 30.3° for the structurally similar octadecanethiol (C18T)[44] SAM. Importantly, the SAM modeled here features naturally occurring domain boundaries and so differs, by design from an idealized, defect-free SAM.[27] As shown in Figure 1, the model features a range of both narrow and broad SAM molecular domain boundaries as well as a central circular Au(111) substrate defect. Note that the "inwards" domain boundary is built by removing two rows of alkanethiols to give a sterically feasible interface of SAM chains with opposing chains oriented "inwards" toward each other. On the other hand, the "outward" domain boundary and the broad "transition" domain boundary were formed with the same local chain density as in the undisturbed SAM regions, that is, no chains were removed.

Following thermal equilibration, the SAM was subjected to 2 ns of free dynamics to allow full structural relaxation in the domain boundary regions and formation of a steady state structure. Uniform distributions of 196, 784, and 3136 free, unbound hexadecanethiol molecules, referred to as excess inks, were subsequently placed on the SAM to give low, medium, and high excess ink concentration systems, yielding total molecule-on-SAM system sizes as large as 994560 atoms, which were subsequently simulated for, in all, over 50 ns (17.5 ns for the low, 30 ns for the medium, and 10 ns for the high concentration system) of dynamics. A reference idealized, defect-free SAM with 784 excess inks was also simulated for 17 ns. Finally a snapshot of the defect SAM with a medium concentration of excess ink molecules at 298 K was taken following 10 ns of dynamics, and the temperature increased to 383 K to produce an additional 5.5 ns high-temperature simulation. Each nanosecond of dynamics took on average approximately 48 h on 512 IBM-BlueGene/P[45] quad-core processors featuring 0.5−1.0 GByte memory per core, for a total simulation time of 80 ns, corresponding to a total computing time of approximately 160 days.

Periodic boundary conditions were applied and Ewald summation used to calculate the electrostatic interactions. Gold atoms were held fixed, and a 2 fs time step used for dynamics by constraining covalent bonds to hydrogen *via* the ShakeH algorithm.[46] The distance between pairs of nonbonded atoms for inclusion in the pair list was set to 13.5 Å with a 12 Å cutoff and a switching function used between 10 and 12 Å. Langevin dynamics was used for heavy atoms with a damping coefficient of 5 ps^{-1}. Velocities were adjusted every 100 ps to remove center of mass motion. The NAMD program,[47] together with the CHARMM22 forcefield,[48] was used for both the room- and high-temperature molecular dynamics with a NVT (constant number of particles, constant volume, and constant temperature) ensemble. This simulation protocol, though using smaller models, was previously shown to[27] (1) produce diffusion coefficients in excellent agreement with experiment for a range of alkanes; (2) reproduce the known SAM tilt angle. Image generation and Tcl script-based trajectory analysis was performed using the VMD program.[49]

Acknowledgment. The research leading to these results has received funding from the European Community's Seventh Framework Programme (FP7/2007-2013) under Grant Agreement No. 213382 (FUNMOL) and Science Foundation Ireland under Grant No. SFI-06/IN.1/I857. Calculations were performed at Tyndall National Institute using computer resources provided by Science Foundation Ireland (SFI), at the SFI/Higher Education Authority Irish Centre for High-End Computing (ICHEC) and also at the IBM Watson Research Center, Yorktown, NY.

Supporting Information Available: A detailed explanation for the formation of broad "transition" SAM domain boundaries. This material is available free of charge *via* the Internet at http://pubs.acs.org.

REFERENCES AND NOTES

1. Love, J. C.; Estroff, L. A.; Kriebel, J. K.; Nuzzo, R. G.; Whitesides, G. M. Self-Assembled Monolayers of Thiolates on Metals as a Form of Nanotechnology. *Chem. Rev.* **2005**, *105*, 1103–1169.
2. Nuzzo, R. G.; Allara, D. L. Adsorption of Bifunctional Organic Disulfides on Gold Surfaces. *J. Am. Chem. Soc.* **1983**, *105*, 4481–4483.
3. Huck, W. T. S. Self-Assembly Meets Nanofabrication: Recent Developments in Microcontact Printing and Dip-Pen Nanolithography. *Angew. Chem., Int. Ed.* **2007**, *46*, 2754–2757.
4. Houseman, B. T.; Huh, J. H.; Kron, S. J.; Mrksich, M. Peptide Chips for the Quantitative Evaluation of Protein Kinase Activity. *Nat. Biotechnol.* **2002**, *20*, 270–274.
5. Jonkheijm, P.; Weinrich, D.; Schroder, H.; Niemeyer, C. M.; Waldmann, H. Chemical Strategies for Generating Protein Biochips. *Angew. Chem., Int. Ed.* **2008**, *47*, 9618–9647.
6. Van Hal, P. A.; Smits, E. C. P.; Geuns, T. C. T.; Akkerman, H. B.; De Brito, B. C.; Perissinotto, S.; Lanzani, G.; Kronemeijer, A. J.; Geskin, V.; Cornil, J.; *et al*. Upscaling, Integration and Electrical Characterization of Molecular Junctions. *Nat. Nanotechnol.* **2008**, *3*, 749–754.
7. Madueno, R.; Raisanen, M. T.; Silien, C.; Buck, M. Functionalizing Hydrogen-Bonded Surface Networks with Self-Assembled Monolayers. *Nature* **2008**, *454*, 618–621.
8. Lee, K. B.; Park, S. J.; Mirkin, C. A.; Smith, J. C.; Mrksich, M. Protein Nanoarrays Generated by Dip-Pen Nanolithography. *Science* **2002**, *295*, 1702–1705.
9. Weiss, P. S.; Mirkin, C. A Conversation with Prof. Chad Mirkin: Nanomaterials Architect. *ACS Nano* **2009**, *3*, 1310–1317.
10. Helmuth, J. A.; Schmid, H.; Stutz, R.; Stemmer, A.; Wolf, H. High-speed Microcontact Printing. *J. Am. Chem. Soc.* **2006**, *128*, 9296–9297.
11. Sharpe, R. B. A.; Titulaer, B. J. F.; Peeters, E.; Burdinski, D.; Huskens, J.; Zandvliet, H. J. W.; Reinhoudt, D. N.; Poelsema, B. Edge Transfer Lithography Using Alkanethiol Inks. *Nano Lett.* **2006**, *6*, 1235–1239.
12. Bumm, L. A.; Arnold, J. J.; Cygan, M. T.; Dunbar, T. D.; Burgin, T. P.; Jones, L.; Allara, D. L.; Tour, J. M.; Weiss, P. S. Are Single Molecular Wires Conducting? *Science* **1996**, *271*, 1705–1707.
13. Wassel, R. A.; Fuierer, R. R.; Kim, N. J.; Gorman, C. B. Stochastic Variation in Conductance on the Nanometer Scale: A General Phenomenon. *Nano Lett.* **2003**, *3*, 1617–1620.
14. Biebuyck, H. A.; Larsen, N. B.; Delamarche, E.; Michel, B. Lithography Beyond Light: Microcontact Printing with Monolayer Resists. *IBM J. Res. Dev.* **1997**, *41*, 159–170.
15. Delamarche, E.; Schmid, H.; Bietsch, A.; Larsen, N. B.; Rothuizen, H.; Michel, B.; Biebuyck, H. Transport Mechanisms of Alkanethiols during Microcontact Printing on Gold. *J. Phys. Chem. B* **1998**, *102*, 3324–3334.
16. Perl, A.; Reinhoudt, D. N.; Huskens, J. Microcontact Printing: Limitations and Achievements. *Adv. Mater.* **2009**, *21*, 2257–2268.
17. Perl, A.; Peter, M.; Ravoo, B. J.; Reinhoudt, D. N.; Huskens, J. Heavyweight Dendritic Inks for Positive Microcontact Printing. *Langmuir* **2006**, *22*, 7568–7573.
18. McDermott, C. A.; McDermott, M. T.; Green, J. B.; Porter, M. D. Structural Origins of the Surface Depressions at Alkanethiolate Monolayers on Au(111)—A Scanning Tunneling and Atomic-Force Microscopic Investigation. *J. Phys. Chem.* **1995**, *99*, 13257–13267.
19. Noh, J.; Hara, M. Molecular-Scale Desorption Processes and the Alternating Missing-Row Phase of Alkanethiol Self-Assembled Monolayers on Au(111). *Langmuir* **2001**, *17*, 7280–7285.
20. Smith, R. K.; Lewis, P. A.; Weiss, P. S. Patterning Self-Assembled Monolayers. *Prog. Surf. Sci.* **2004**, *75*, 1–68.
21. Godin, M.; Williams, P. J.; Tabard-Cossa, V.; Laroche, O.; Beaulieu, L. Y.; Lennox, R. B.; Grutter, P. Surface Stress, Kinetics, and Structure of Alkanethiol Self-Assembled Monolayers. *Langmuir* **2004**, *20*, 7090–7096.
22. Vericat, C.; Vela, M. E.; Salvarezza, R. C. Self-Assembled Monolayers of Alkanethiols on Au(111): Surface Structures, Defects and Dynamics. *Phys. Chem. Chem. Phys.* **2005**, *7*, 3258–3268.
23. O'Dwyer, C.; Gay, G.; de Lesegno, B. V.; Weiner, J. The Nature of Alkanethiol Self-Assembled Monolayer Adsorption on Sputtered Gold Substrates. *Langmuir* **2004**, *20*, 8172–8182.
24. Gronbeck, H.; Curioni, A.; Andreoni, W. Thiols and Disulfides on the Au(111) Surface: The Headgroup−Gold Interaction. *J. Am. Chem. Soc.* **2000**, *122*, 3839–3842.
25. Vemparala, S.; Karki, B. B.; Kalia, R. K.; Nakano, A.; Vashishta, P. Large-Scale Molecular Dynamics Simulations of Alkanethiol Self-Assembled Monolayers. *J. Chem. Phys.* **2004**, *121*, 4323–4330.
26. Prathima, N.; Harini, A.; Rai, N.; Chandrashekara, R. H.; Ayappa, K. G.; Sampath, S.; Biswas, S. K. Thermal Study of Accumulation of Conformational Disorders in the Self-Assembled Monolayers of C-8 and C-18 Alkanethiols on the Au(111) Surface. *Langmuir* **2005**, *21*, 2364–2374.
27. Gannon, G.; Larsson, J. A.; Greer, J. C.; Thompson, D. Quantification of Ink Diffusion in Microcontact Printing with Self-Assembled Monolayers. *Langmuir* **2009**, *25*, 242–247.
28. Schonenberger, C.; Sondaghuethorst, J. A. M.; Jorritsma, J.; Fokkink, L. G. J. What Are the "Holes" in Self-Assembled Monolayers of Alkanethiols on Gold. *Langmuir* **1994**, *10*, 611–614.
29. Schonenberger, C.; Jorritsma, J.; Sondaghuethorst, J. A. M.; Fokkink, L. G. J. Domain Structure of Self-Assembled Alkanethiol Monolayers on Gold. *J. Phys. Chem.* **1995**, *99*, 3259–3271.
30. Poirier, G. E. Characterization of Organosulfur Molecular Monolayers on Au(111) Using Scanning Tunneling Microscopy. *Chem. Rev.* **1997**, *97*, 1117–1127.
31. Yamada, R.; Wano, H.; Uosaki, K. Effect of Temperature on Structure of the Self-Assembled Monolayer of Decanethiol on Au(111) Surface. *Langmuir* **2000**, *16*, 5523–5525.
32. Munuera, C.; Barrena, E.; Ocal, C. Deciphering Structural Domains of Alkanethiol Self-Assembled Configurations by Friction Force Microscopy. *J. Phys. Chem. A* **2007**, *111*, 12721–12726.
33. Srinivasan, C.; Mullen, T. J.; Hohman, J. N.; Anderson, M. E.; Dameron, A. A.; Andrews, A. M.; Dickey, E. C.; Horn, M. W.; Weiss, P. S. Scanning Electron Microscopy of Nanoscale Chemical Patterns. *ACS Nano* **2007**, *1*, 191–201.
34. Kind, M.; Woll, C. Organic Surfaces Exposed by Self-Assembled Organothiol Monolayers: Preparation, Characterization, and Application. *Prog. Surf. Sci.* **2009**, *84*, 230–278.
35. Donhauser, Z. J.; Mantooth, B. A.; Kelly, K. F.; Bumm, L. A.; Monnell, J. D.; Stapleton, J. J.; Price, D. W.; Rawlett, A. M.; Allara, D. L.; Tour, J. M.; *et al*. Conductance Switching in Single Molecules through Conformational Changes. *Science* **2001**, *292*, 2303–2307.
36. Zhang, H. J.; Huang, H.; He, P. M.; Bao, S. N.; Zhou, W. Z.; Richardson, N. V. Transportation of Molecules with a Scanning Tunneling Microscope. *Appl. Phys. Lett.* **2006**, *89*, 3.
37. Schwartz, P.; Schreiber, F.; Eisenberger, P.; Scoles, G. Growth Kinetics of Decanethiol Monolayers Self-Assembled on Au(111) by Molecular Beam Deposition: An Atomic Beam Diffraction Study. *Surf. Sci.* **1999**, *423*, 208–224.
38. Jung, L. S.; Campbell, C. T. Sticking Probabilities in Adsorption of Alkanethiols from Liquid Ethanol Solution onto Gold. *J. Phys. Chem. B* **2000**, *104*, 11168–11178.
39. Schreiber, F. Structure and Growth of Self-Assembling Monolayers. *Prog. Surf. Sci.* **2000**, *65*, 151–256.
40. Ulman, A. Formation and Structure of Self-Assembled Monolayers. *Chem. Rev.* **1996**, *96*, 1533–1554.
41. O'Dwyer, C. *In-Situ* Examination of the Selective Etching of an Alkanethiol Monolayer Covered Au{111} Surface. *Mater. Lett.* **2007**, *61*, 3837–3841.

42. Dameron, A. A.; Hampton, J. R.; Smith, R. K.; Mullen, T. J.; Gillmor, S. D.; Weiss, P. S. Microdisplacement Printing. *Nano. Lett.* **2005**, *5*, 1834–1837.
43. Mullen, T. J.; Srinivasan, C.; Hohman, J. N.; Gillmor, S. D.; Shuster, M. J.; Horn, M. W.; Andrews, A. M.; Weiss, P. S. Microcontact Insertion Printing. *Appl. Phys. Lett.* **2007**, *90*, 063114.
44. Fenter, P.; Eisenberger, P.; Liang, K. S. Chain-Length Dependence of the Structures and Phases of $CH_3(CH_2)_{n-1}$ SH Self-Assembled on Au(111). *Phys. Rev. Lett.* **1993**, *70*, 2447–2450.
45. Almasi, G.; Asaad, S.; Bellofatto, R. E.; Bickford, H. R.; Blumrich, M. A.; Brezzo, B.; Bright, A. A.; Brunheroto, J. R.; Castanos, J. G.; Chen, D.; *et al*. Overview of the IBM Blue Gene/P project. *IBM J. Res. Dev.* **2008**, *52*, 199–220.
46. Ryckaert, J. P.; Ciccotti, G.; Berendsen, H. J. C. Numerical-Integration of Cartesian Equations of Motion of a System with Constraints—Molecular-Dynamics of *n*-Alkanes. *J. Comput. Phys.* **1977**, *23*, 327–341.
47. Phillips, J. C.; Braun, R.; Wang, W.; Gumbart, J.; Tajkhorshid, E.; Villa, E.; Chipot, C.; Skeel, R. D.; Kale, L.; Schulten, K. Scalable Molecular Dynamics with NAMD. *J. Comput. Chem.* **2005**, *26*, 1781–1802.
48. MacKerell, A. D.; Bashford, D.; Bellott, M.; Dunbrack, R. L.; Evanseck, J. D.; Field, M. J.; Fischer, S.; Gao, J.; Guo, H.; Ha, S.; *et al*. All-Atom Empirical Potential for Molecular Modeling and Dynamics Studies of Proteins. *J. Phys. Chem. B* **1998**, *102*, 3586–3616.
49. Humphrey, W.; Dalke, A.; Schulten, K. VMD: Visual Molecular Dynamics. *J. Mol. Graph.* **1996**, *14*, 33–38.